


Article

Simulation and Optimization of Shot Peening Process for CoCrFeNiAlx High-Entropy Alloy

Xiaodong Li ¹, Guoqing Gou ^{2,*}, Chuanhai Jiang ^{1,*} and Jijin Xu ¹ 

¹ School of Materials Science and Engineering, Shanghai Jiaotong University, Shanghai 200240, China; lixiaodong@casic.com.cn (X.L.)

² Key Laboratory of Advanced Materials Technology Ministry of Education, Southwest Jiaotong University, Chengdu 610031, China

* Correspondence: gouguoqing1001@163.com (G.G.); chjiang@sjtu.edu.cn (C.J.)

Abstract: In this work, Ti-10V-2Fe-3Al alloy was selected as the test material, and the shot peening process of a CoCrFeNiAlx system high-entropy alloy was simulated based on effective test conditions, and the effects of dry shot peening and wet shot peening on the surface properties were determined. Preliminary simulation results the surface of the test sample display a clear plastic deformation state that gradually diminishes and shifts towards the outermost layer. The stress transfer of the test sample gradually decreases, showing a gradient change, and the twin density also shows a random sample change. Then, the high-entropy alloy shot peening process was optimized, and the best process parameters were determined by analyzing the microhardness data, depth of action layer, and surface state. It was found that after wet shot peening, a new characteristic peak is generated, and with the increase in the size of the shot, its overall kinetic energy becomes increasingly higher, the strain energy of the material surface becomes increasingly higher, and the grain refinement is relatively high. This work provides a new approach to investigating the issues that are present during the shot peening process of CoCrFeNiAlx system high-entropy alloys.

Keywords: CoCrFeNiAlx system; high entropy; alloy; shot peening; technology; simulation; optimization



Citation: Li, X.; Gou, G.; Jiang, C.; Xu, J. Simulation and Optimization of Shot Peening Process for CoCrFeNiAlx High-Entropy Alloy. *Metals* **2023**, *13*, 1537. <https://doi.org/10.3390/met13091537>

Academic Editor: Miroslav Zivkovic

Received: 1 July 2023

Revised: 17 August 2023

Accepted: 21 August 2023

Published: 30 August 2023



Copyright: © 2023 by the authors. Licensee MDPI, Basel, Switzerland. This article is an open access article distributed under the terms and conditions of the Creative Commons Attribution (CC BY) license (<https://creativecommons.org/licenses/by/4.0/>).

1. Introduction

There are several methods to enhance the hardness of metals, such as decreasing the grain size, implementing a multilayer system, or utilizing shot peening. One approach is to reduce the grain size through processes like severe plastic deformation or grain refinement techniques [1–3]. By decreasing the grain size, the material's strength and hardness can be significantly increased due to the limited movement of dislocations within smaller grains. Another strategy involves creating a multilayer system where alternating layers of different materials or varying grain sizes are stacked together [4,5]. This can induce a barrier effect and hinder dislocation movement, leading to improved hardness [6]. Additionally, shot peening, a surface treatment technique, involves bombarding the metal surface with high-velocity spherical particles. This process induces plastic deformation, generating compressive residual stresses and work hardening, resulting in increased hardness and improved mechanical properties [7]. These approaches offer effective means to enhance the hardness of metals, enabling their application in various industries such as the automotive, aerospace, and tooling industries. Shot peening is a common strengthening process which mainly uses the principle of stress implantation to bombard the surface of materials and improve the basic properties of materials [8,9]. Therefore, shot peening is also a cold processing process. After shot peening, the materials not only have increased wear resistance, but also corrosion resistance and fatigue resistance. The device used for shot peening is simple, so the cost is relatively low and the limitation is small [10–12]. Common shot peening includes cast steel shot, cast iron shot, glass shot, etc. Shot peening is a shot peening

strengthening process, which mainly focuses on dealing with the fatigue of materials. The objective is to extend the lifespan of materials and minimize material waste. During this process, the exterior of materials will undergo certain plastic changes, forming a relatively reliable strengthened surface, which can offset the load of materials and reduce the fatigue risk of materials. Therefore, it is widely used in various parts' processing.

Alloy is a common metal material, and high-entropy alloy is a special high-performance alloy, which is mainly formed by more than five metals and has relatively ideal performances [13–15]. CoCrFeNiAlx high-entropy alloy is a kind of high-entropy alloy. Its tensile strength and fracture resistance are better than conventional alloys, but the overall strength still needs to be improved. With the change in service conditions of the CoCrFeNiAlx system high-entropy alloy, its mechanical properties will also change correspondingly, which will affect the service life of the CoCrFeNiAlx system high-entropy alloy [16–19]. Therefore, the shot peening strengthening of CoCrFeNiAlx system high-entropy alloy is an important means to improve its service properties.

The CoCrFeNiAlx system high-entropy alloy has high strength, and it is difficult for shot peening to form an effective strengthened surface layer, as it can only introduce relatively strong compressive stress. The shot peening methods that are currently in use consist of primary and secondary processes, as well as thermal techniques, dry and wet shot peening processes, etc. During treatment, the residual stress may not change significantly due to the change in surface composite force [20–23]. The comprehensive properties of CoCrFeNiAlx high-entropy alloys have not been significantly enhanced. Therefore, in order to improve the shot peening effect of CoCrFeNiAlx system high-entropy alloys and solve the existing shot peening problem [24–26], this paper simulates the shot peening process of CoCrFeNiAlx system high-entropy alloys, optimizes the original shot peening process through orthogonal tests, obtains the optimal process parameters, and makes a certain contribution to improving the comprehensive performance of the alloy.

Generally, the failure behavior of metal materials begins on the surface of structural components, and when the fatigue failure of the material surface is damaged, cracks and expansion of the structural surface first appear, resulting in the final fracture of the material and in reduced equipment life and major accidents. Therefore, the strengthening of the surface properties of the material structure can significantly increase the service life of the material. The shot peening process is a cost-effective technical means to improve the surface performance of materials that continuously sprays the surface of the workpiece material at room temperature through high-speed fine steel shot flow, so that the surface of the workpiece has different degrees of cyclic elastoplastic deformation according to the process requirements, so as to introduce the required residual compressive stress within a certain depth of the material surface. At the same time, shot peening can effectively refine the crystals of the hardened layer, and improve the degree of microdistortion and dislocation density of the surface layer of the material. The results show that this residual compressive stress strengthening and microstructure strengthening can effectively limit the dislocation movement and inhibit or slow down the initiation and propagation of microcracks. However, for high-entropy alloys with a single-phase structure, the shot peening mechanism has not been systematically studied. Therefore, based on the shot peening simulation calculation and experimental verification, the shot peening strengthening process and mechanical properties of the material are studied, and the influence mechanism of shot peening strength on the residual stress of the structure is analyzed, which is of great significance for the shot peening process to efficiently improve the hardness and yield strength of the material and improve the surface fatigue performance of the material.

Nowadays, the service environment of aerospace, automotive, mechanical equipment, and other industries is becoming more and more stringent, and its performance requirements have increased sharply. The requirements for the strength and surface quality of the corresponding parts are also becoming higher and higher. Therefore, based on economic cost and performance stability, component surface treatment has become an indispensable and important process. At present, shot peening technology is one of the simplest and most

effective ways to improve the surface quality of mechanical parts, which can significantly improve the fatigue life of the workpiece surface, is not limited by the position and shape of the workpiece, and is widely used in various industrial fields. However, shot peening is a complex cold working process involving static and dynamic elasticity, plasticity, and other disciplines and has more adjustable process parameters because shot peening involves impact problems, resulting in the whole process also needing to consider the corresponding workpiece stability, Baussinger effect, material inertia, and other issues. Among them, the process parameters mainly involve material parameters (such as material model of the projectile and workpiece) and shot peening process parameters (such as projectile size, shot peening speed, etc.). However, the current theoretical research on shot peening analysis is still incomplete. In particular, the analysis of its mechanism has not been fully explained, so simulation calculation will help to carry out refined process parameter regulation and intensification.

With the rapid development of finite element methods and computer technology, many numerical models based on finite element methods to study shot peening residual stress have emerged. Meguid et al. [27] and Majzoubi et al. [28] used a three-dimensional multi-pellet symmetry model to systematically analyze the shot peening process. By simulating multiple impacts on the target plate at different speeds, the residual compressive stress distribution on the surface of the material was obtained, and the effects of speed and shot peening coverage were studied. Meo et al. analyzed the residual stress distribution generated by the finite element method to simulate the welding area of a single projectile impact workpiece using the finite element method, and the results show that the residual compressive stress generated by shot peening reduces the tensile stress generated by the welding process, which is the same as the actual result, thus proving the feasibility of analyzing the shot peening process using the finite element method.

In the past, the determination of shot peening process parameters was mainly performed through the finite element calculation simulation of the macroscopic pattern and the comparison of the shot peening experiment. In this paper, the influence of dry and wet shot peening on the surface properties was determined by focusing on the microscopic characterization, and the characterization and orthogonal test simulation analyses were used to optimize the high-entropy alloy shot peening process and determine the best process parameters. The novelty of this study lies in a different focus. Since all our previous research groups conducted shot peening studies, there are not many references from teachers and peers. This paper mainly analyzes and compares results from the orthogonal experiment and microscopic level, and the focus is different from previous studies. The simulation process is described in detail in the form of orthogonal experimental data expressed in a table. Roughness and microhardness are not the focus of this paper because the microhardness data, layer depth, and surface state are mainly introduced in this paper. In this paper, the simulation process and results are presented in the form of orthogonal experiments.

2. Simulation of Shot Peening Process for CoCrFeNiAl_x High-Entropy Alloy

In combination with the requirements for the shot peening simulation of CoCrFeNiAl_x system high-entropy alloy, Ti-10V-2Fe-3Al alloy is chosen as the experimental material for this study. Table 1 below displays the chemical composition of the experimental material.

Table 1. Chemical composition of experimental materials.

Element	Content (wt%)
N	0.03
O	0.03
H	0.01
Al	3.42
V	8.16
Fe	2.12
Ti	remain

It can be seen from Table 1 that according to the chemical composition of the above simulated experimental materials, they can be effectively cut. In this paper, the high entropy alloy is cut into a sample that meets the observation requirements using the electric spark cutting method, and a unified heat treatment process is carried out to obtain a consistent micro-shot peening fabric [29]. The heat treatment's temperature is kept at 830 °C, and the oil quenching treatment is carried out for 20 min to generate a single β phase structure. At this time, the sample structure is relatively coarse, which does not meet the requirements of shot peening process simulation. It needs to be polished to remove the oxide film and polished to a smooth shot peening surface.

Conventional high-entropy alloy shot peening mainly includes dry shot peening and wet shot peening. After many pre-experiments, it is found that the surface integrity of dry shot peening is relatively low [30–32], and the shot peening effect is poor. Therefore, this paper uses two shot peening methods for high-entropy alloy shot peening. The ratio of wet shot peening to water is 1:10, and a 6050 B sandblasting machine is selected as the shot peening machine. Its parameters are shown in Table 2 below.

Table 2. Parameters of 6050 B sandblasting machine.

Option	Parameter
External dimensions	1000 mm × 1600 mm × 1700 mm
Working window size	1000 mm × 800 mm × 830 mm
Number of spray guns	2 (aluminum alloy guns with boron carbide nozzles)
Dust removal power	550 W (according to the sand material configuration used)
Each processing volume	15–20 kg (optimal sandblasting workload)
Dust removal box	1 set (bag type pneumatic dust removal can also be selected with filter element dust removal or wet dust removal)
Air source requirements	The air compressor is required to be above 15 KW
Power supply	380 V/50 HZ

It can be seen from Table 2 that the 6050 B sandblasting machine has good performance and can carry out automatic sandblasting, which meets the requirements of high-entropy alloy shot peening process simulation. After preliminary shot peening, it is found that the integrity of the surface of the experimental sample material has improved, and the effect is still difficult to guarantee. In addition, the effect of shot peening process simulation may change due to the impact of the pressure, distance, and other parameters of shot peening. Therefore, this paper uses constant shot peening pressure to simulate the shot peening process, and always keeps the shot peening distance at 30 mm.

After shot peening, vertically cut the selected Ti-10V-2Fe-3Al alloy sample, select a treatment surface as the observation area, polish and polish, prepare corrosion solution for corrosion, and observe the surface morphology of the test sample [33]. In this paper, Nova Nano SEM450 is selected as the observation microscope, and JEM-2010HT is used for shot peening strengthening impact analysis to prepare TEM test samples. To measure the variation in surface roughness of the samples before and after shot peening, this paper preset the sampling speed, and the roughness calculation formula at this time R_a is shown in Formula (1) below [34].

$$R_a = \frac{1}{l} \int_0^l |y(x)| dx \quad (1)$$

In Formula (1), $y(x)$ represents the distance from the surface contour of the sample to each centerline, dx represents the arithmetic mean of the contour, and l represents the sampling length.

Combined with the above simulation observation tools, the generated shot peening process simulation samples can be processed, and the metallographic structure of the section can be intercepted at 10 min, as shown in Figure 1 below.

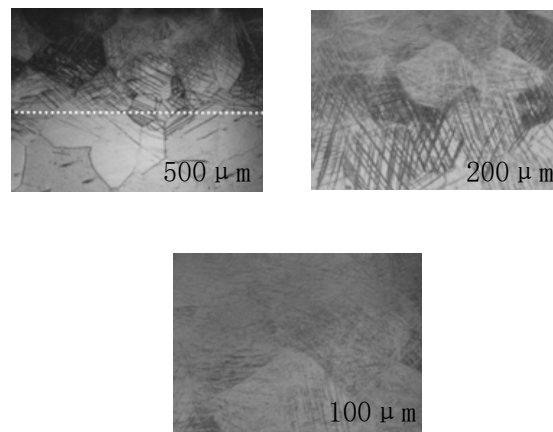


Figure 1. Metallographic structure of section.

It can be seen from Figure 1 that after shot peening, the surface of the test sample displays a clear plastic deformation state that gradually diminishes and shifts towards the outermost layer. It can be seen that the stress transfer of the test sample gradually decreases, showing a gradient change, and the twin density also shows a random sample change.

As the shot peening time increases, the surface penetration depth on the sample gradually expands. At this time, the surface of the sample gradually shows plastic deformation, resulting in a rheological phenomenon. At this time, the microstructure of the shot-peened Ti-10V-2Fe-3AL alloy sample is shown in Figure 2 below.

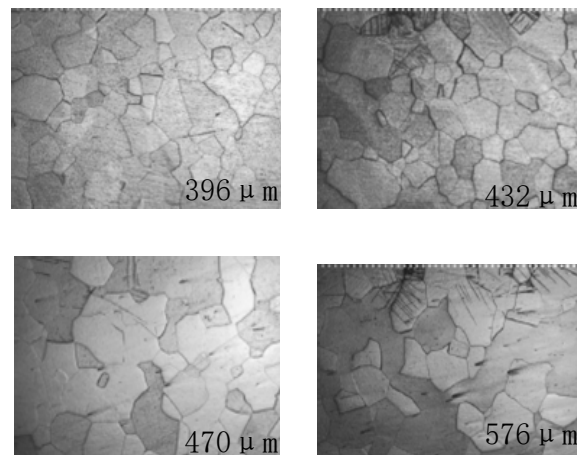


Figure 2. Ti-10V-2Fe-3AL alloy sample structure.

It can be seen from Figure 2 that, as the shot peening time increases, the shot peening action depth gradually deepens and results in a relatively smooth surface flatness of the sample. It can be seen that wet shot peening can effectively protect the smoothness of the sample. When the shot peening process was carried out for 5 min, a white bright layer appeared on the surface of the sample, and the original grain boundary began to be blurred [35]. As the shot peening time continued to increase, the area of the white area became larger and larger, which proved that the area was related to the size of the shot peening kinetic energy, and the shot peening damage of the test material was relatively reduced due to the buffer effect of the wet shot peening water medium.

As the shot peening time of Ti-10V-2Fe-3AL alloy sample increases, the overall depth of shot peening also gradually increases. It can be seen that the depth of the action layer of shot peening is related to the kinetic energy of the shot to some extent. At this time, the depth time change in the wet shot peening action layer is shown in Table 3 below.

Table 3. Depth time variation in shot peening action layer.

Implementation Time of Shot Peening Process (min)	Depth of Shot Peening Action Layer (μm)
10	250
20	260
30	270
40	275
50	279
60	282
70	283
80	284
90	285
100	286

It can be seen from Table 3 that as the shot peening time increases, the depth of the shot peening action layer becomes larger and larger and maintains a slow growth trend after reaching a certain depth.

In the process of high-entropy alloy shot peening, the surface microstructure of the sample will change to varying degrees. Therefore, when conducting surface RXD analysis, the dislocation density of the sample can be calculated ρ , as shown in (2) below.

$$\rho = rl \quad (2)$$

In Formula (2), r represents the micro-fine particle size. At this time, X-ray diffraction is carried out to analyze the alteration in the stress state of the sample structure, and the surface layer XRD pattern is generated. At this time, the phase angle of the sample composition is singular. After wet shot peening, a new characteristic peak is generated. It can be seen from the XRD spectrum that the increase in time may lead to the distortion of the sample surface, and the dislocation density continues to increase.

Analyze the microscopic morphology of the sample, use SEM to scan the surface morphology of the sample, and observe the SEM structures of different projectile size sections, as shown in Figure 3 below.

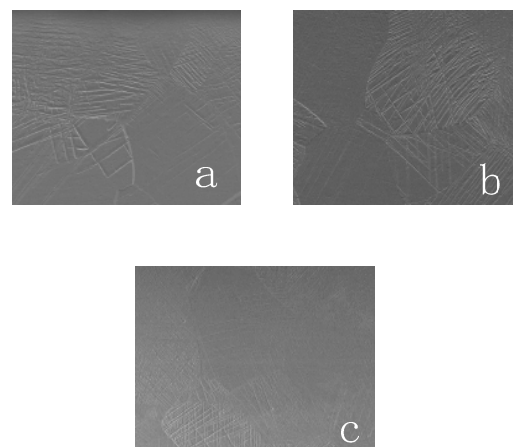


Figure 3. Surface morphology of SEM scanning samples with different shot peening sizes. (a) 1 mm, (b) 2 mm and (c) 3 mm.

It can be seen from Figure 3 that when the shot peening time does not change, with the increase in the size of the shot, its overall kinetic energy is increasingly higher, the strain energy of the material surface is increasingly higher, and the grain refinement is relatively high. In the process of shot peening strengthening, the impact speed of the shot is relatively high, which can easily cause deformation on the surface of the test material. From the energy point of view, the kinetic energy carried by the shot after acceleration is relatively

high, and the transformed strain energy is also relatively high. Therefore, with the increase in the kinetic energy of the shot, the depth of the working layer of shot peening is also becoming higher and higher.

3. Optimization of Shot Peening Process for 2CoCrFeNiAlx High-Entropy Alloy

Combined with the above simulation process of the CoCrFeNiAlx system high-entropy alloy shot peening process, the shot peening process can be optimized. Because the microstructure and properties of dry and wet shot peening samples have changed to varying degrees, the orthogonal test method is used to optimize the shot peening process by combining the extreme value and variance of shot peening process parameters to obtain the best shot peening process parameters.

An orthogonal test can effectively deal with the influencing factors of the shot peening process, and simple experimental steps are used to determine the optimal process state. In this paper, from the three aspects of deformation layer depth, roughness, and microhardness, shot peening size and time parameters are selected for orthogonal testing. Table 4 below displays the factor levels used in the orthogonal test.

Table 4. Orthogonal test factor level table.

Level	Dry Shot Size (mm)	Dry Shot Peening Time (min)	Wet Shot Peening Size (mm)	Wet Shot Peening Time (min)
1	1	15	2	15
2	3	25	1	35
3	2	20	4	5
4	4	30	3	25

It can be seen from Table 4 that the orthogonal test mainly takes the depth of the action layer, the surface roughness of the sample, and the microhardness as the main analysis indicators. A total of 16 tests were conducted to optimize the final experimental results. The orthogonal test design table and the orthogonal test results at this time are displayed in Table 5 below.

Table 5. Orthogonal test design table and results.

Group	Dry Shot Size (mm)	Empty Column	Dry Shot Peening Time (min)	Wet Shot Peening Size (mm)	Wet Shot Peening Time (min)	Depth of Action Layer (μm)	Roughness (μm)	Microhardness (HV)
G1	1	1	15	2	15	749	0.788	401.5
G2	1	2	25	1	35	413	0.792	407.1
G3	1	3	20	4	5	793	0.611	397.2
G4	1	4	30	3	25	89	0.598	406.25
G5	2	1	25	4	25	1194	0.582	398.25
G6	2	2	15	3	5	919	0.574	382.5
G7	2	3	30	2	35	840	0.682	410.6
G8	2	4	20	1	15	730	0.762	364.7
G9	3	1	20	3	35	1186	0.598	361
G10	3	2	30	4	15	1390	0.714	365.1
G11	3	3	15	1	25	1041	0.570	387
G12	3	4	25	2	5	1467	0.670	380
G13	4	1	30	1	5	1146	0.773	369.4
G14	4	2	20	2	25	1291	0.624	395.5
G15	4	3	25	3	15	1258	0.654	358.2
G16	4	4	15	4	35	1468	0.728	360.3

It can be seen from Table 5 that according to the test results obtained in the above table, range analysis can be conducted to evaluate the influence of various factors on the shot peening process by visual analysis R , as shown in Formula (3) below [36].

$$R = K_{\max} - K_{\min} \quad (3)$$

In Formula (3), K_{\max} represents the maximum range and K_{\min} represents the minimum range. For different factors having different effects on the process, the primary and secondary factors are set in this paper, and the shot peening time is adjusted [37]. At this time, the orthogonal test results are visually analyzed, as shown in Table 6 below.

Table 6. Orthogonal test results.

Index	K Value	Dry Shot Size (mm)	Empty Column	Dry Shot Size (mm)	Wet Shot Peening Size (mm)	Wet Shot Peening Time (min)
Depth of deformation layer (μm)	K1	2844	4275	4177	4347	4127
	K2	3683	4013	4332	3330	3907
	K3	5084	3932	4000	4845	4325
	K4	5163	4554	4265	4252	4415
	k1	711	1068.75	1044.25	1086.75	1031.75
	k2	920.75	1003.25	1083	832.5	976.75
	k3	1271	983	1000	1211.25	1081.25
	k4	1290.75	1138.5	1066.25	1063	1103.75
	range R	2319	622	265	1515	508
Roughness	K1	2.789	2.741	2.66	2.764	2.918
	K2	2.6	2.704	2.698	2.897	2.8
	K3	2.552	2.517	2.595	2.635	2.628
	K4	2.779	2.758	2.767	2.424	2.374
	k1	0.69725	0.68525	0.665	0.691	0.7295
	k2	0.65	0.676	0.6745	0.72425	0.7
	k3	0.638	0.62925	0.64875	0.65875	0.657
	k4	0.69475	0.6895	0.69175	0.606	0.5935
	range R	0.237	0.241	0.172	0.473	0.544
Microhardness (HV)	K1	1612	1530.1	1531.3	1587.6	1489.5
	K2	1556	1550.2	1543.5	1528.2	1539
	K3	1493.1	1553	1548.4	1520.8	1529.1
	K4	1483.4	1511.2	1551.3	1507.9	1586.9
	k1	403	382.525	382.825	396.9	372.375
	k2	389	387.55	385.875	382.05	384.75
	k3	373.275	388.25	379.6	380.2	382.275
	k4	370.85	377.8	387.825	376.975	396.725
	range R	128.6	41.8	32.9	79.7	97.4

It can be seen from Table 6 that, combined with the above table, the impact of various factors on the shot peening process indicators can be estimated, and the final optimization scheme can be obtained. In order to further judge the significance relationship between the shot peening process parameters and the shot peening layer, the depth variance analysis is conducted in this paper, and the analysis results are shown in Table 7 below.

Table 7. Results of deep variance analysis.

Source of Variance	Sum of Squares of Deviations	Freedom	Mean Square	Variance
Dry shot peening dimension A	0.011	3	0.0037	1.693
Dry shot peening time B	0.0039	3	0.0013	
Wet shot size C	0.0304	3	0.0101	4.62
Wet shot peening time D	0.0418	3	0.0140	6
Error deviation	0.0092	3	0.003	
New error deviation	0.0131	6	0.00218	

It can be seen from Table 7 that the impact of the dry shot peening time on sample roughness is relatively low, and the secondary items can be regarded as error items. At this time, the dry shot peening time can be fixed for size verification. The results show that the microhardness and roughness are good when the dry shot peening size is 4 mm. After the above steps are completed, the dry shot peening size can be fixed to determine the optimal wet shot peening attribute. The results show that when the wet shot peening size is 2 mm, it is in the optimal state.

Once the dry and wet shot peening sizes are chosen, the shot peening time parameters need to be optimized and the dry and wet shot peening sizes need to be fixed. At this time, it can be concluded that the shot peening performance is best when the wet shot peening and dry shot peening time is 25 min. The above optimization parameters are verified, and the results show that the selected shot peening size and time meet the requirements of micro hardness, depth of action layer and surface state of shot peening, and are reliable, which proves that the shot peening optimization parameters set in this paper have certain application value [38–40].

4. Conclusions

In this paper, the conventional high-entropy alloy shot peening process of CoCrFeNiAl_x system is simulated, the existing process problems are analyzed, and the effective optimization is carried out, which makes a certain contribution to optimizing the comprehensive properties of metal materials. It is mainly optimized by the best process parameters. Through 16 experiments, the optimization results are finally obtained. The results show that when the shot peening size is 4 mm, the microhardness and roughness of the alloy are good, and when the wet shot peening size is 2 mm, the alloy is in the best state. The results indicate that the effect of shot peening process simulation may change due to the impact of the pressure, distance, and other parameters of shot peening. Simulation results indicate the surface of the test sample displays a clear plastic deformation state that gradually diminishes and shifts towards the outermost layer. The stress transfer of the test sample gradually decreases, showing a gradient change, and the twin density also shows a random sample change. After wet shot peening, a new characteristic peak is generated. Meanwhile, with the increase in the size of the shot, its overall kinetic energy is increasingly higher, the strain energy of the material surface is increasingly higher, and the grain refinement is relatively high. Therefore, this paper simulates the conventional high-entropy alloy shot peening process of the CoCrFeNiAl_x system, analyzes the existing process problems, and effectively optimizes them, which makes a certain contribution to optimizing the comprehensive properties of metal materials. This paper will conduct further research on the basis of the present findings.

Author Contributions: Conceptualization, X.L.; Software, X.L. and J.X.; Validation, X.L. and J.X.; Investigation, J.X.; Resources, G.G.; Writing—original draft, X.L.; Writing—review and editing, G.G.; Visualization, J.X.; Supervision, C.J.; Project administration, C.J.; Funding acquisition, C.J. All authors have read and agreed to the published version of the manuscript.

Funding: This research was funded by Fundamental Research Funds for the Central Universities grant numbers 2682022ZTPY003, 2682022CX021, 2682021GF023, 2682022ZTPY090, and 2682022ZK051.

Data Availability Statement: Not applicable.

Acknowledgments: This work was supported by Fundamental Research Funds for the Central Universities (Grant Nos. 2682022ZTPY003, 2682022CX021, 2682021GF023, 2682022ZTPY090, and 2682022ZK051).

Conflicts of Interest: The authors declare no conflict of interest.

References

1. Tajudin, M.F.M.; Ahmad, A.H.; Alias, J.; Razak, N.A.A.; Alang, N.A. Grain refinement in semi-solid metal processing: Current status and recent development. *Int. J. Adv. Manuf. Technol.* **2023**, *124*, 1379–1399. [\[CrossRef\]](#)
2. Haghayeghi, R.; Zoqui, E.J.; Bahai, H. An investigation on the effect of intensive shearing on the grain refinement of A5754 aluminium alloy. *J. Alloys Compd.* **2009**, *481*, 358–364. [\[CrossRef\]](#)
3. Li, K.; He, Y.; Fang, C.; Ma, H.; Kim, J.; Lee, H.S.; Song, J.I.; Yang, C.W.; Lee, J.H.; Shin, K. Surface nanocrystallization of pure Cu induced by ultrasonic shot peening. *J. Nanosci. Nanotechnol.* **2014**, *14*, 9637–9643. [\[CrossRef\]](#)
4. Panchenko, I.; Wolter, K.J.; Croes, K.; De Wolf, I.; De Messemaeker, J.; Beyne, E.; Wolf, M.J. Effects of isothermal storage on grain structure of Cu/Sn/Cu microbump interconnects for 3D stacking. *Microelectron. Reliab.* **2019**, *102*, 113296. [\[CrossRef\]](#)
5. Huang, E.W.; Lee, W.J.; Singh, S.S.; Kumar, P.; Lee, C.Y.; Lam, T.N.; Chin, H.H.; Lin, B.H.; Liaw, P.K. Machine-learning and high-throughput studies for high-entropy materials. *Mater. Sci. Eng. R Rep.* **2022**, *147*, 100645. [\[CrossRef\]](#)
6. AlMotasem, A.T.; Daghbouj, N.; Sen, H.S.; Mirzaei, S.; Callisti, M.; Polcar, T. Influence of HCP/BCC interface orientation on the tribological behavior of Zr/Nb multilayer during nanoscratch: A combined experimental and atomistic study. *Acta Mater.* **2023**, *249*, 118832. [\[CrossRef\]](#)
7. Kattoura, M. Effects of Advanced Surface Treatments on the Fatigue Behavior of ATI 718Plus at Room and Elevated Temperatures. Ph.D. Dissertation, University of Cincinnati, Cincinnati, OH, USA, 2017.
8. Daghbouj, N.; Sen, H.S.; Čížek, J.; Lorinčík, J.; Karlík, M.; Callisti, M.; Čech, J.; Havránek, V.; Li, B.; Krsjak, V.; et al. Characterizing heavy ions-irradiated Zr/Nb: Structure and mechanical properties. *Mater. Des.* **2022**, *219*, 110732. [\[CrossRef\]](#)
9. Daghbouj, N.; Sen, H.S.; Callisti, M.; Vronka, M.; Karlík, M.; Duchoň, J.; Čech, J.; Havránek, V.; Polcar, T. Revealing nanoscale strain mechanisms in ion-irradiated multilayers. *Acta Mater.* **2022**, *229*, 117807. [\[CrossRef\]](#)
10. Ye, C.; Telang, A.; Gill, A.S.; Suslov, S.; Idell, Y.; Zwiack, K.; Wiezorek, J.M.K.; Zhou, Z.; Qian, D.; Mannava, S.R.; et al. Gradient nanostructure and residual stresses induced by Ultrasonic Nano-crystal Surface Modification in 304 austenitic stainless steel for high strength and high ductility. *Mater. Sci. Eng. A* **2014**, *613*, 274–288. [\[CrossRef\]](#)
11. Shivpuri, R.; Cheng, X.; Mao, Y. Elasto-plastic pseudo-dynamic numerical model for the design of shot peening process parameters. *Mater. Des.* **2009**, *30*, 3112–3120. [\[CrossRef\]](#)
12. Samoilova, O.; Shaburova, N.; Samodurova, M.; Pashkeev, K.; Moghaddam, A.O.; Doubenskaia, M.; Sova, A.; Trofimov, E. Microstructural evolution of Al_{0.25}CoCrFeNiCu and Al_{0.45}CoCrFeNiSi_{0.45} high-entropy alloys during laser cladding. *Proc. Inst. Mech. Eng. Part L J. Mater. Des. Appl.* **2022**, *236*, 1806–1813. [\[CrossRef\]](#)
13. Tsuru, T.; Lobzenko, I.; Wei, D. Synergetic effect of Si addition on mechanical properties in face-centered-cubic high entropy alloys: A first-principles study. *Model. Simul. Mater. Sci. Eng.* **2022**, *30*, 024003. [\[CrossRef\]](#)
14. Hu, J.; Zhang, J.; Li, M.; Zhang, S.; Xiao, H.; Xie, L.; Sun, G.; Shen, H.; Zhou, X.; Li, X.; et al. The origin of anomalous hydrogen occupation in high entropy alloys. *J. Mater. Chem. A* **2022**, *10*, 7228–7237. [\[CrossRef\]](#)
15. Chong, Z.; Sun, Y.; Cheng, W.; Han, C.; Su, C.; Nafitha, D.; Fan, Z. Effect of Nano WC on Wear and Corrosion Resistances of AlCoCrFeNi High-entropy Alloy Coating. *Cailiao Daobao/Mater. Rep.* **2022**, *33*, 104417. [\[CrossRef\]](#)
16. Sorkin, V.; Tan, T.L.; Yu, Z.G.; Zhang, Y.W. High-throughput calculations based on the small set of ordered structures method for non-equimolar high entropy alloys. *Comput. Mater. Sci.* **2021**, *188*, 110213. [\[CrossRef\]](#)
17. Huang, L.; Wang, X.; Jia, F.; Zhao, X.; Huang, B.; Ma, J.; Wang, C. Effect of Si element on phase transformation and mechanical properties for FeCoCrNiSix high entropy alloys. *Mater. Lett.* **2021**, *282*, 128809. [\[CrossRef\]](#)
18. Kolodiy, I.V.; Velikodnyi, O.M.; Tikhonovsky, M.A.; Voyevodin, V.N.; Kalchenko, O.S.; Vasilenko, R.L.; Okovit, V.S. Microstructure and Mechanical Properties of Oxide Dispersion Strengthened High-Entropy Alloys Cocrfemni and CrFe₂MnNi. *Probl. At. Sci. Technol.* **2021**, *87–94*. [\[CrossRef\]](#)
19. Bhandari, U.; Ghadimi, H.; Zhang, C.; Gao, F.; Yang, S.; Guo, S. Computational exploration of biomedical HfNbTaTiZr and Hf_{0.5}Nb_{0.5}Ta_{0.5}Ti_{1.5}Zr refractory high-entropy alloys. *Mater. Res. Express* **2021**, *8*, 096534. [\[CrossRef\]](#)
20. Liu, X.; Jia, N.; Chen, S.; Wang, L.; Ke, H.; Jin, K.; Wang, B.; Wang, L.; Fan, Q.; Xue, Y. Method to identify the phase structures of high entropy alloys with modified lattice distortion enthalpy. *Mater. Today Commun.* **2021**, *29*, 102760. [\[CrossRef\]](#)
21. Astafurova, E.G.; Panchenko, M.Y.; Reunova, K.A.; Mikhno, A.S.; Moskvina, V.A.; Melnikov, E.V.; Astafurov, S.V.; Maier, H.J. The effect of nitrogen alloying on hydrogen-assisted plastic deformation and fracture in FeMnNiCoCr high-entropy alloys. *Scr. Mater.* **2020**, *194*, 113642. [\[CrossRef\]](#)
22. Xie, T.; Jin, F.; Qin, J.; Qin, L.; Long, S.; Yi, Y.; Zhou, S. Effects of La and Y on the microstructure and mechanical properties of NbMoTiVSi_{0.3} refractory high entropy alloys. *J. Alloys Compd.* **2023**, *931*, 167464. [\[CrossRef\]](#)
23. Shaysultanov, D.G.; Raimov, K.S.; Stepanov, N.D. Effect of carbon content, deformation and annealing on the structure and properties of interstitial TRIP high-entropy alloys. *IOP Conf. Ser. Mater. Sci. Eng.* **2021**, *1014*, 012052. [\[CrossRef\]](#)
24. Chen, S.; Wang, L.; Wang, L.; Xue, Y.; Wang, B. Enhanced phase stability of a BCC structure system high-entropy alloys by decreasing elastic distortion energy. *J. Phys. Conf. Ser.* **2021**, *1948*, 012207. [\[CrossRef\]](#)
25. Lu, Z.P.; Wang, H.; Chen, M.W.; Baker, I.; Yeh, J.W.; Liu, C.T.; Nieh, T.G. An assessment on the future development of high-entropy alloys: Summary from a recent workshop. *Intermetallics* **2015**, *66*, 67–76. [\[CrossRef\]](#)
26. Irizalp, S.G.; Koroglu, B.K.; Sokol, D. Influence of Laser Peening with and Without Coating on the Surface Properties and Stress Corrosion Cracking Behavior of Laser-Welded 304 Stainless Steel. *Metall. Mater. Trans. A Phys. Metall. Mater. Sci.* **2021**, *52*, 3302–3316. [\[CrossRef\]](#)

27. Meguid, S.A.; Shagal, G.; Stranart, J.C.; Daly, J. Three-dimensional dynamic finite element analysis of shot-peening induced residual stresses. *Finite Elem. Anal. Des.* **1999**, *31*, 179–191. [[CrossRef](#)]
28. Majzooobi, G.H.; Azizi, R.; Alavi Nia, A. A three-dimensional simulation of shot peening process using multiple shot impacts. *J. Mater. Process. Technol.* **2005**, *146*, 1226–1234. [[CrossRef](#)]
29. Sun, Y.; Lan, A.; Zhang, M.; Yang, H.; Qiao, J. Influence of lanthanum on passivity behavior of CrMnFeNi high entropy alloys. *Mater. Chem. Phys.* **2021**, *265*, 124509. [[CrossRef](#)]
30. Edalati, K.; Li, H.W.; Kilmametov, A.; Floriano, R.; Borchers, C. High-pressure torsion for synthesis of high-entropy alloys. *Metals* **2021**, *11*, 1263. [[CrossRef](#)]
31. Huang, S.; Wu, H.; Zhu, H.; Xie, Z. Effect of niobium addition upon microstructure and tensile properties of CrMnFeCoNi_x high entropy alloys. *Mater. Sci. Eng. A* **2021**, *809*, 140959. [[CrossRef](#)]
32. Zhu, C.Y.; Wu, H.; Zhu, H.G.; Li, X.D.; Tu, C.L.; Xie, Z.H. Mechanical properties and fracture mechanism of as-cast MnFeCoCuNi_x high-entropy alloys. *Trans. Nonferrous Met. Soc. China (Engl. Ed.)* **2021**, *31*, 222–231. [[CrossRef](#)]
33. Ondicho, I.; Alunda, B.; Park, N. Effect of Fe on the Hall-Petch relationship of (CoCrMnNi)_{100-x} Fe_x medium-and high-entropy alloys. *Intermetallics* **2021**, *136*, 107239. [[CrossRef](#)]
34. Xiao, Q.; Wang, L.; Liang, Y.J.; Xue, Y. Annealing hardening in cryo-rolled high-entropy alloys by belated deformation twinning. *Mater. Sci. Eng. A* **2021**, *801*, 140403. [[CrossRef](#)]
35. Zeng, Y.; Man, M.; Bai, K.; Zhang, Y.W. Revealing high-fidelity phase selection rules for high entropy alloys: A combined CALPHAD and machine learning study. *Mater. Des.* **2021**, *202*, 109532. [[CrossRef](#)]
36. Hashimoto, N.; Ono, Y. Mobility of point defects in CoCrFeNi-base high entropy alloys. *Intermetallics* **2021**, *133*, 107182. [[CrossRef](#)]
37. Liu, J.; Xu, J.; Sleiman, S.; Chen, X.; Zhu, S.; Cheng, H.; Huot, J. Microstructure and hydrogen storage properties of Ti–V–Cr based BCC-type high entropy alloys. *Int. J. Hydrogen Energy* **2021**, *46*, 28709–28718. [[CrossRef](#)]
38. Liu, H.; Dong, H.; Tang, J.; Ding, H.; Shao, W.; Zhao, J.; Jiang, T. Numerical modeling and experimental verification of surface roughness of 12Cr2Ni4Al alloy steel generated by shot peening. *Surf. Coat. Technol.* **2021**, *422*, 127538. [[CrossRef](#)]
39. Liu, H.C.; Tsai, C.W. Effect of Ge addition on the microstructure, mechanical properties, and corrosion behavior of CoCrFeNi high-entropy alloys. *Intermetallics* **2021**, *132*, 107167. [[CrossRef](#)]
40. Li, L.; Chang, H.; Pares, J.M.; Bradák, B.; Zhang, Z.; Qiang, X.; Guan, C.; Quan, C. Cenozoic Uplift of Tanggula Range and Tuouohe Basin. Northern Tibet: Insights of the Anisotropy of Magnetic Susceptibility. *Front. Earth Sci.* **2022**, *10*, 815315. [[CrossRef](#)]

Disclaimer/Publisher’s Note: The statements, opinions and data contained in all publications are solely those of the individual author(s) and contributor(s) and not of MDPI and/or the editor(s). MDPI and/or the editor(s) disclaim responsibility for any injury to people or property resulting from any ideas, methods, instructions or products referred to in the content.